

THE DEGRADATION OF THE PROTECTIVE SCALE ON BINARY FeCr ALLOYS (Fe-2.25Cr, Fe-10Cr, Fe-18Cr AND Fe-25Cr) IN CO₂ AND IN CO₂ + H₂O ENVIRONMENT AT 600°C

DEGRADASI LAPISAN OKSIDA PROTEKTIF DARI PADUAN FeCr (Fe-2,25Cr, Fe-10Cr, Fe-18Cr AND Fe-25Cr) DI LINGKUNGAN O₂ DAN O₂ + H₂O PADA TEMPERATUR 600°C

Bagas Pujilaksono

Engineering Faculty, Gadjah Mada University

Graduate School, Gadjah Mada University

Email: Bagas.pujilaksono@ugm.ac.id

First Registered on March 8th 2016; Received after Correction on April 8th 2016

Publication Approval on: April 29th 2016

ABSTRAK

Perilaku oksidasi dari paduan logam Fe-2,25Cr, Fe-10Cr, Fe-18Cr dan Fe-25Cr diinvestigasi pada kondisi kering dan basah pada temperatur 600°C. Eksperimen dilakukan dengan cara oksidasi isothermal hingga 168 jam pada sampel yang telah dipolis secara sempurna. Lapisan oksida yang terbentuk diinvestigasi secara gravimetri dan dianalisa dengan X-ray diffraction, dan X-ray photoelectron spectroscopy untuk analisa profil elemen pada kedalaman. Morfologi dari oksida pada permukaan diinvestigasi dengan SEM. Tampang lintang oksida dianalisa dengan SEM/EDX untuk mendapatkan gambar dan komposisi kimia. Perilaku oksidasi dari paduan FeCr terletak antara besi dan krom. Fe-2.25Cr sangat mirip dengan besi pada kedua kondisi lingkungan, yaitu terbentuk lapisan non-protektif yang terdiri dari FeCr spinel di dasar oksida, magnetit di tengah dan hematit di bagian atas. Pada kondisi O₂ kering, Fe-10Cr, Fe-18Cr, dan Fe-25Cr membentuk lapisan oksida protektif (Fe,Cr)₂O₃ yang mirip dengan kromia yang terbentuk pada oksidasi krom. Pada kondisi O₂ basah, awalnya Fe-10Cr, Fe-18Cr, dan Fe-25Cr membentuk lapisan oksida protektif seperti pada kondisi kering. Namun setelah selang beberapa waktu oksidasi, dimana sangat tergantung kandungan krom, semua ketiga paduan logam tersebut mengalami breakaway oxidation, dan membentuk lapisan oksida non-protektif yang mirip dengan lapisan oksida pada Fe-2.25Cr. Breakaway oxidation pada kondisi O₂ basah dipicu terjadinya evaporasi CrO₂(OH)₂ dari lapisan pasif (Fe,Cr)₂O₃.

Kata Kunci: efek uap air, evaporasi kromia, oksida protektif, breakaway oxidation

ABSTRACT

The oxidation behaviour of the binary alloys Fe-2.25, Fe-10Cr, Fe-18Cr and Fe-25Cr in dry and wet O₂ at 600°C is investigated by isothermal exposures of carefully polished samples for up to 168 hours. The oxidized samples are investigated gravimetrically and the oxides formed are studied by X-ray diffraction. X-ray photoelectron spectroscopy is used for depth profiling of the thin oxides. The scale surface is imaged by SEM. Cross sections through the scale are analyzed by SEM/EDX for imaging and for measuring the chemical composition. The oxidation behavior of the four FeCr alloys is intermediate between those of iron and chromium. Fe-2.25Cr oxidizes in a way similar to iron in both environments, forming a poorly protective scale consisting of FeCr spinel at the bottom, magnetite in the middle and a hematite cap layer. In dry O₂, Fe-10Cr, Fe-18Cr and Fe-25Cr form a thin and protective (Fe,Cr)₂O₃ oxide similar to the chromia film formed on pure chromium. In wet O₂, Fe-10Cr, Fe-18Cr and Fe-25Cr initially form the same kind of protective oxide film as in dry conditions. After an incubation time that depends on alloy chromium content, all three alloys go into breakaway oxidation and form thick, poorly protective scales

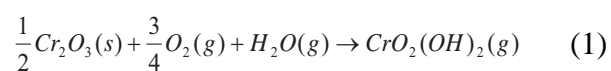
similar to those formed on Fe-2.25Cr. Breakaway oxidation in wet O₂ is triggered by the evaporation of CrO₂(OH)₂ from the protective (Fe,Cr)₂O₃ oxide.

Keywords: water vapour effect, chromia vaporization, protective oxide, breakaway oxidation

I. INTRODUCTION

Iron based alloys are frequently used at high temperature. At moderate temperature (say <500 °C) and “clean” environments, low alloyed steels are often preferred. In that temperature range, low alloyed steels form an oxide scale consisting of hematite Fe₂O₃ and magnetite Fe₃O₄ which has sufficient protective properties for many applications. At higher temperature and in “dirty” environments, the rate of oxidation becomes too great and the low alloyed steels are replaced by stainless steels (iron based alloys with >9% Cr). The ability of stainless steels to resist oxidation at high temperature relies on the formation of corundum type chromium-rich solid solution of hematite and chromium oxide (Cr_xFe_{1-x})₂O₃ (x<0.5) and iron chromium spinel oxide Fe(Fe_{1-x}Cr_x)₂O₄ (x>0.5). Because of the great importance of these materials in high temperature applications there are a great number of publications concerning their oxidation properties. The literature in the field is summarized by Kofstad and Birks & Meier.

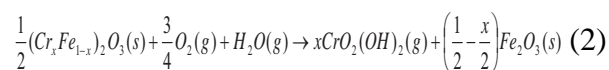
In many cases it has been reported that water vapor increases the rate of stainless steel oxidation at high temperature (Kofstad 1988 & Birks et al. 2006). The influence of water vapor in the presence of O₂ on the oxidation of pure iron at 400-600°C was recently investigated at this laboratory (Opila et al. 2007). At 400°C, a small oxidation inhibiting effect was found which was attributed to competition between the adsorption of water and O₂ on the scale surface. At 500 and 600°C, water vapor was found to accelerate oxidation somewhat. This effect was attributed to changes in the microstructure of the hematite layer. In the case of pure chromium, exposure to mixtures of O₂ and H₂O at high temperature results in the vaporization of chromium (VI) oxide hydroxide:



Source: Opila et al.

The competition between the parabolic growth of Cr₂O₃ and the (constant rate) vaporization of CrO₂(OH)₂ results in so-called para-linear kinetics, the TG curve bending downwards and oxide thickness tending towards a constant value (Pujilaksono et al. 2008 & Tedmon 1966). Vaporization of chromium (VI) oxide hydroxide also affects stainless steel in environments containing O₂+ H₂O at high

temperature (Asteman 2002, Astemen 2000 & Hansel 2003).



The vaporization of chromia from the scale tends to convert the protective chromium-rich oxide to hematite, resulting in a loss of protective properties. The acceleration of stainless steel oxidation by water vapour in the presence of O₂ has been attributed to this effect. Thus, the effect of chromia vaporization on stainless steel oxidation has been shown to depend on the relation between the rate of supply of chromia to the scale and on the rate of chromia vaporization (Asteman 2002 & Astemen 2000). The importance of the chromium vaporization rate is illustrated by the strong influence of gas velocity on the oxidation of FeCrNi steels in H₂O + O₂ environment at 600°C (Hansel 2003). At low gas velocities, the rate of chromia vaporization was not sufficient to trigger a breakdown of the protective oxide. At high gas velocity, the rate of chromia loss was not compensated by Cr diffusion from the alloy, resulting in a Cr depletion of the corundum type oxide and causing breakaway oxidation.

At low oxygen activities, reactions (1) and (2) are of no importance and the acceleration of stainless steel oxidation by water vapour in reducing environment must have other causes. Various explanations have been suggested for the effect of water vapour in reducing conditions. For example, Tveten et al. suggest that exposure to water vapour results in the take-up of protons which influences the defect equilibria and thereby the transport properties of the oxide.

The present paper addresses the effect of water vapour in the presence of O₂ on the oxidation of four binary FeCr alloys (Fe-2.25Cr, Fe-10Cr, Fe-18Cr, Fe-25Cr) at 600°C. To contribute to the fundamental understanding of the water vapour effect, the study involves model alloys rather than commercial stainless steels. In this way we eliminate the influence of other alloying elements and alloy microstructure on oxidation. The exposed materials are investigated with respect to oxidation kinetics and the oxides formed are characterized by a combination of techniques. The morphology and elemental composition of the oxide is investigated by SEM-EDX imaging in plan view and of polished

cross sections. The phase composition of oxide is studied by X-ray diffraction and XPS is used for providing compositional depth profiles of the thin, protective oxide.

II. EXPERIMENTAL

A. Materials

The Fe-Cr model alloys (Fe-2.25Cr, Fe-10.0Cr, Fe-18.0Cr and Fe-25.0Cr) were prepared by Sandvik Materials Technology AB. The materials were produced by hot extrusion in order to achieve a homogenous grain structure. The grain diameter was in the range 50-300µm. The alloy composition is given in Table 1. Sample coupons were cut to size (15.0x15.0x2.0 mm), mechanically ground in ethanol to 4000 mesh on SiC paper and polished with 1.0 µm diamond paste to mirror finish. After polishing the samples were cleaned successively in ethanol,

acetone and ethanol for 10 minutes using ultrasonic agitation. The samples were then dried and stored in a desiccator over P₂O₅ awaiting exposure.

B. Oxidation Exposures

Isothermal oxidation exposures were carried out using a horizontal furnace fitted with a 45 mm (inner diameter) SiO₂- glass tube. The samples were exposed three at a time using a sample holder made from sintered alumina. The coupons were positioned parallel to the direction of the gas flow. The samples were exposed for 1, 24 and 168 hours. Each sample was only exposed to high temperature once, *i.e.*, the samples were not put back into the furnace after weighing. The mass changes were recorded using a microbalance with 1µg resolution. The mass gains are averages of triplicate samples. The scatter in mass gain was less than 2% or < 0.002 mg/cm². The exposure gas consisted of 95%N₂+5%O₂ (termed

Table 1
Alloy composition (wt. %)

Element	Fe-2.25Cr	Fe-10Cr	Fe-18Cr	Fe-25Cr
C	0.005	0.006	0.006	0.006
Si	0.01	0.02	0.03	0.03
Mn	0.02	0.03	0.03	0.03
P	0.003	0.004	0.004	0.004
S	0.005	0.005	0.005	0.005
Cr	2.26	10.43	18.08	25.00
Ni	0.01	0.01	0.01	0.01
Mo	0.01	0.01	0.01	0.01
Co	0.01	0.01	0.01	0.01
Cu	0.010	0.010	0.010	0.010
Sn	0.002	0.002	0.003	0.003
As	0.003	0.003	0.003	0.003
B	0.0000	0.0001	0.0002	0.0002
Ti	0.02	0.02	0.02	0.02
Al	0.02	0.02	0.02	0.02
Nb	0.01	0.01	0.01	0.01
Ta	<0.01	<0.01	<0.01	<0.01
Zr	0.005	0.004	0.004	0.004
Pb	0.0001	0.0002	0.0003	0.0003
Bi	0.00003	0.00005	0.00007	0.00007
O	100-200 ppm	100-200 ppm	100-200 ppm	100-200 ppm
N	0.002	0.004	0.006	0.006
Fe	balance	balance	balance	balance

“dry O₂“ below) or 5% O₂+40% H₂O+55% N₂ (termed “wet O₂“ below). The water vapour content was achieved by saturating the gas with water vapour at the desired dew point. To avoid condensation, the temperature in the exposure system was kept above the dew point of the gas. In the dry O₂ exposures the water concentration was about 5 ppm. The experiment was started by putting the holder with the samples into the hot furnace. This operation took ~30 seconds. After exposure the samples were removed from the hot zone within 30 seconds and were then allowed to cool in dry air.

C. Analytical Techniques

X-ray diffraction (XRD)

Scale composition was investigated by X-ray diffraction. A Siemens D5000 powder X-ray diffractometer equipped with grazing incidence beam attachment and a Göbel mirror was used. Measurements were carried out in the Grazing Incidence (GI-XRD) and Bragg-Brentano (BB-XRD) geometry using CuK_{α1} radiation. In the GI-XRD measurements the angle of incidence was 0.3-10 degrees. The Sol-X detector measured between 20.0° till 65.0°.

Analytical Scanning Electron Microscopy (SEM/EDX)

An FEI Quanta 200 ESEM (Environmental Scanning Electron Microscope) equipped with a field emission gun (FEG) was used. Accelerating voltage of 10-15 kV, high vacuum mode and 10 mm working distance were chosen. Secondary electron (SE) and backscattered electron (BSE) modes have been used. Chemical analysis was carried out using an Oxford INCA Energy Dispersive X-ray (EDX) system.

X-ray Photoelectron Spectroscopy (XPS)

XPS was used to perform elemental depth profiling of the scale. XPS measurements were performed in a Perkin Elmer XPS (model PHI 5500) apparatus at a base pressure 1×10^{-7} Pa. AlK α radiation (1486.6 eV), was used and the emitted photoelectrons were analyzed with 23.5 eV pass energy. The spectrometer was calibrated using copper, silver and gold standards, and all spectra were corrected with respect to energy calibration and carbon peak shift due to removal of hydroxide contamination. The C1s peak position of the as-prepared material (285.5 eV) was used as reference. For XPS depth profiling, the sample was sputtered by a 4 kV Ar⁺ ion beam with an angle of incidence of 50°. The ion beam scanned an area of 3x4 mm².

Sputter depth was estimated using the sputter rate of Ta₂O₅. Peak de-convolution and background spectra subtraction was done by using Multipak© software, using external standards of pure chromium and pure iron. In the present study there was no indication of charging of the samples.

III. RESULTS

A. Mass Gain in Dry and Wet O₂

The mass gain of Fe-2.25Cr at 600°C in dry and wet O₂ is shown in Fig.1. Mass gain is roughly parabolic in both environments, the parabolic rate constant (k') being approximately $5 \cdot 10^{-11}$ (g²/cm⁴s) in dry O₂ and $1.4 \cdot 10^{-10}$ (g²/cm⁴s) in wet O₂. Hence, the rate of oxidation is increased in the presence of water vapour. All samples exposed in the presence of water vapour experienced exfoliation of the scale

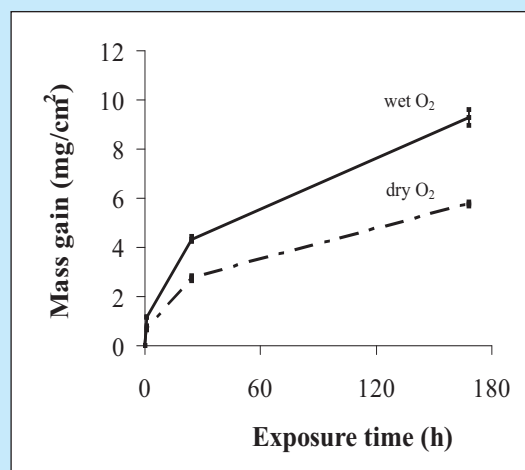


Figure 1
Mass gain of Fe-2.25Cr at 600 °C in dry O₂ (lower curve) and wet O₂ (upper curve). The lines are just guides to the eye.

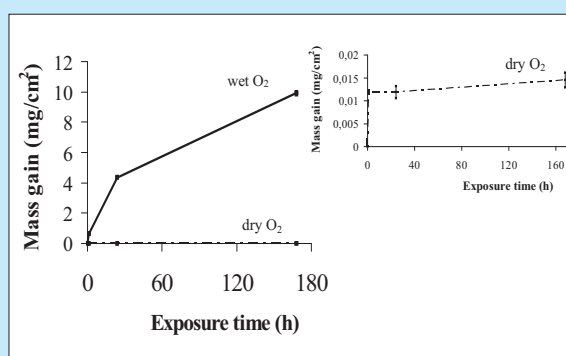


Figure 2
Mass gain of Fe-10Cr at 600 °C in dry O₂ and wet O₂. The lines are just guides to the eye.

during cooling. The mass gain of Fe-10Cr in dry and wet O₂ at 600°C is shown in Fig.2. In dry O₂, mass gain is very small, indicating the formation of a protective oxide. Kinetics are sub-parabolic, mass gain being small after the first hour. In contrast, exposure to wet O₂ resulted in large mass gains also after 1 hour, reflecting the break-down of the protective oxide by water vapour. In fact, the mass gain curve of Fe-10Cr in wet O₂ is almost the same as that of Fe-2.25Cr. The mass gain of Fe-18Cr at 600°C in dry and wet O₂ is shown in Fig.3. As for Fe-10Cr, the mass gain in dry O₂ is very small, the alloy showing protective behaviour and sub-parabolic kinetics. In the presence of water vapour the alloy behaves in a peculiar manner, showing very low mass gain and protective behaviour up to one hour exposure time and large mass gains and non-protective behaviour after 24 and 168 hours. Again, once breakaway has occurred the mass gain curve is similar to (but slightly below) that of Fe-2.25Cr. The mass gain of Fe-25Cr at 600°C in dry and wet O₂ is shown in Fig.4. As for Fe-10Cr and Fe-18Cr, this alloy also exhibits protective behaviour in dry O₂ with very small mass gains and sub-parabolic kinetics. The oxidation behaviour in wet O₂ is similar to that of Fe-18Cr, the alloy going from protective to non-protective behaviour after a certain exposure time. In the case of Fe-25Cr, the alloy stays in the protective state up to 24 hours but has gone into breakaway oxidation after 168 hours exposure. In this case, the mass gain after 168 hours in wet O₂ (after breakaway has occurred) is about 25% of the value for Fe-2.25Cr. An inspection of Fig. 4 shows that the TG curve in wet O₂ has a negative slope between 1 and 24 hours exposure time, *i.e.*, before breakaway. This is attributed to the evaporation of chromia (see discussion). According to the gravimetric data the oxidation behaviour of the samples fall into two categories; 1) slow mass gain (sometimes even a slight mass loss), corresponding to a thin and protective oxide (average thickness is below about 0.1µm) and or rapid mass gain, corresponding to a poorly protective oxide (the average oxide thickness is in the range 5-50µm). The mass gain results are summarized in Table 2:

B. Phase Composition of the Scale in Dry and Wet O₂

The XRD analyses of the exposed samples are summarized in Table 3. Fig. 5 shows a Grazing incidence XRD (GI-XRD) diffractogram of Fe-2.25Cr after 24 hours exposure in dry O₂. Hematite

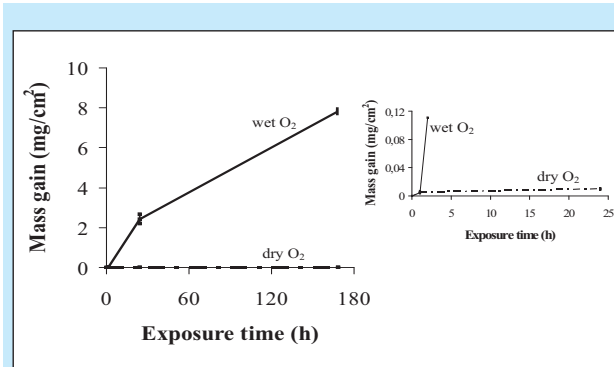


Figure 3
Oxidation kinetics of Fe-18Cr at 600°C in dry and wet O₂.

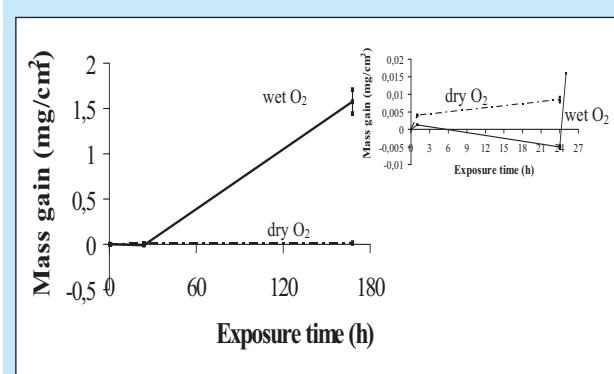


Figure 4
Mass gain of Fe-25Cr at 600°C in dry and wet O₂.

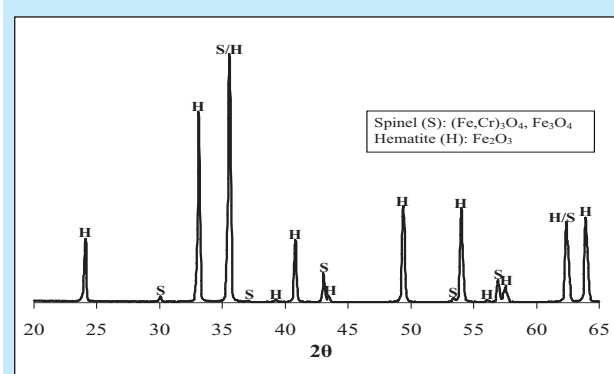


Figure 5
GI-XRD diffractogram of Fe-2.25Cr after 24 hours exposure in dry O₂ at 600°C.

and spinel oxide were identified. Due to peak overlap, it was not possible to distinguish magnetite and (Fe, Cr)₃O₄. However, SEM/EDX cross section analysis showed the presence of both Fe₃O₄ and (Fe, Cr)₃O₄ (see Fig. 13. below). Fig. 6 shows GI-XRD diffractograms of Fe-10Cr, Fe-18Cr and Fe-25Cr after 168 hours in dry O₂. All three diffractograms

Table 2
Summary of mass gain results at 600°C (mg/cm²)*

Alloy Comp.	Dry O ₂			Wet O ₂		
	1 hour	24 hours	168 hours	1 hour	24 hours	168 hours
Fe-2.25Cr	0.723	2.753	5.755	1.159	4.333	9.276
Fe-10Cr	0.012	0.012	0.015	0.637	4.362	9.908
Fe-18Cr	0.005	0.010	0.012	0.005	2.433	7.844
Fe-25Cr	0.004	0.008	0.014	0.001	-0.005	1.574

*If we make the approximation that the oxides are dense and assume that chromia vaporization can be neglected, mass gain is easily converted into average oxide thickness. When mass gain is small (0.015 mg/cm² and below), only (Fe,Cr)₂O₃ forms and the oxide thickness (in μm) is computed by multiplying mass gain (in mg/cm²) by the factor 6.2. When mass gain is large, several oxides are present. The corresponding multiplying factor for magnetite and iron chromium spinel is 7.0 while it is 6.4 for hematite. Due to chromia vaporization, the small mass gains in wet O₂ do not give reliable estimates of the thickness of the thin oxide.

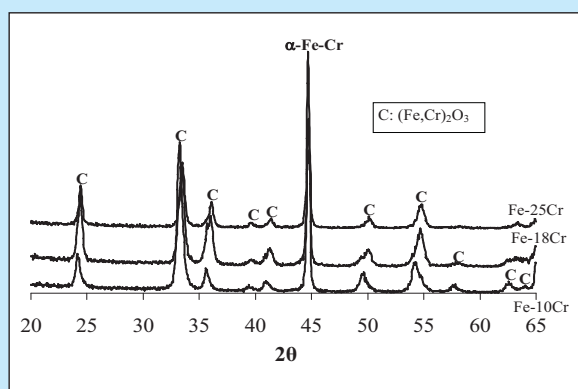


Figure 6
GI-XRD diffractograms of Fe-10Cr, Fe-18Cr and Fe-25Cr after 168 hours exposure in dry O₂.

show that corundum type (Fe,Cr)₂O₃ is the only oxide formed. The exact position of the XRD peaks depends on alloy composition, corresponding to an increase in the chromium content of (Fe, Cr)₂O₃ as the Cr content in the alloy increases (see Fig. 7). As noted above, exposure to wet O₂ triggered rapid oxidation in several cases (See Table 2 and 3). However, exposure of Fe-18Cr for one hour and exposure of Fe-25 for up to 24 hours did not result in rapid oxidation. In those cases XRD analysis indicated the same phase composition as in dry O₂, the diffractograms in Fig. 8 showing the presence of (Fe, Cr)₂O₃ on the samples. After longer exposure times when breakaway oxidation occurred, (compare Table 2 and 3) the protective (Fe, Cr)₂O₃ is replaced by a combination of hematite and spinel, the lack of signal for the substrate indicating the presence of a thick scale. (see Fig. 9).

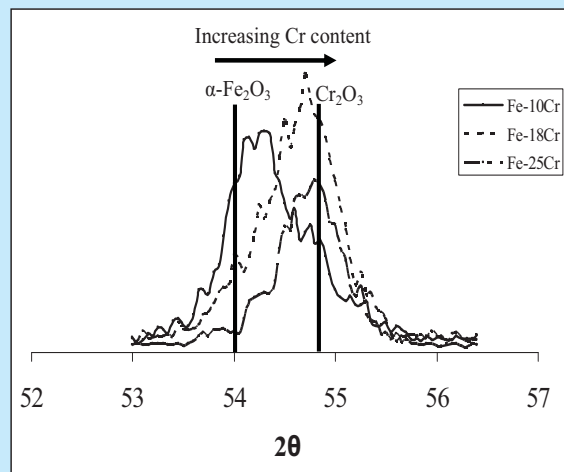


Figure 7
The (Fe,Cr)₂O₃ (1 1 6) peak on Fe-10Cr, Fe-18Cr and Fe-25Cr after 168 hours exposure in dry O₂. The peak position depends on the chromium content of the oxide. The oxide formed on Fe-25Cr and Fe-18Cr has peak positions close to that of Cr₂O₃ while Fe-10Cr exhibits a peak position corresponding to a more iron-rich average composition of the oxide.

C. XPS Analysis of the Thin and Protective Oxide After Exposure in Dry and wet O₂

XPS analysis of the exposed samples showed no unexpected elements. The outermost 5 nm were excluded from the depth profiles because the oxide surface was contaminated due to handling in air. The average thickness of the protective oxide in dry O₂ (calculated from the mass gain, see Table 2) ranged from about 30nm after one hour to about 100nm after 168 hours. The identification of corundum

type oxide by XRD on all samples exhibiting a thin and protective oxide allows us to interpret the XPS results in terms of (Fe,Cr)₂O₃. The results of the XPS analysis are summarized in Table 4. Figure 10 shows an XPS depth profile acquired from Fe-18Cr after 1 hour in dry O₂ at 600°C, showing the distribution of Fe (metal), Cr (metal), Fe (oxide) and Cr (oxide). The chromia concentration increases as the scale/metal interface is approached, the composition changing from about (Fe_{0.7}Cr_{0.2})₂O₃ close to the scale surface to about (Fe_{0.4}Cr_{0.6})₂O₃ close to the scale/metal interface. The depth profiles acquired from the protective oxides formed on Fe-10Cr and Fe-25Cr in dry O₂ were similar to those shown in

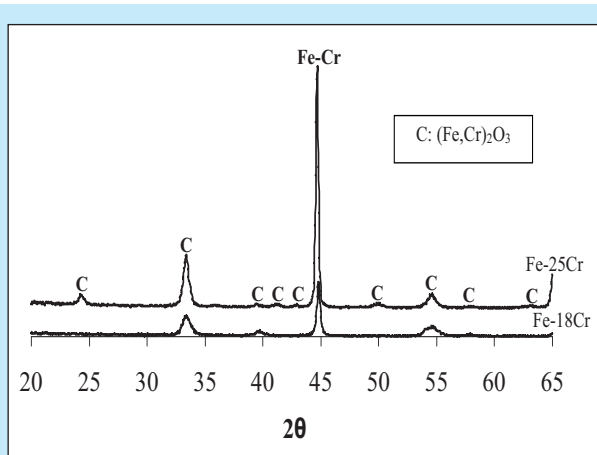


Figure 8
GI-XRD diffractogram of Fe-18Cr (1 hour) and Fe-25Cr (24 hours) at 600°C in wet O₂.

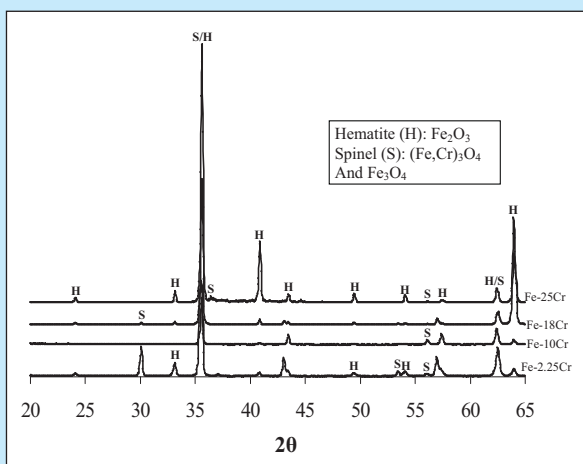


Figure 9
BB-XRD diffractograms of Fe-2.25Cr (24 hours), Fe-10Cr (24 hours), Fe-18Cr (24 hours) and Fe-25Cr (168 hours) after oxidation in wet O₂ at 600°C. All samples had formed a thick scale (compare Table 2).

Fig.10 for Fe-18Cr. The main difference is that the chromium concentration in the oxide is correlated to the chromium concentration in the alloy (see Table 4). Figure 11 shows an XPS depth profile of the protective oxide formed on Fe-18Cr after 1 hour of exposure in wet O₂ at 600 °C. In comparison to the corresponding dry exposure (Fig.10), the oxide close to the surface has a lower Cr/Fe ratio corresponding to a mixed oxide with the approximate composition (Fe_{0.8}Cr_{0.2})₂O₃. As in the dry run, the chromium content in the oxide increases as we go deeper into the oxide. The only other observations of thin and protective oxides in wet oxygen were made on Fe-

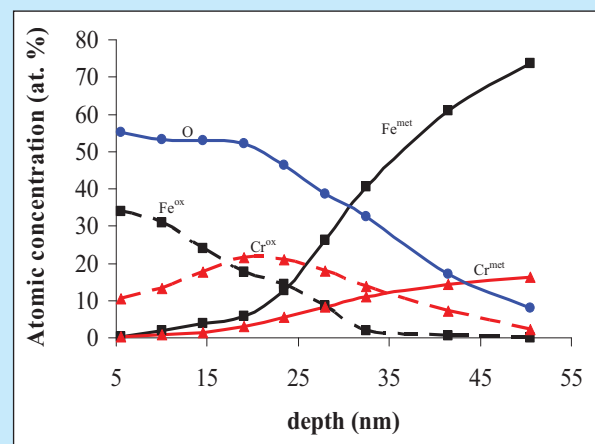


Figure 10
XPS depth profile of Fe-18Cr after 1 hour exposure in dry O₂ at 600°C showing the elemental distribution of O, Fe^{met}, Fe^{ox}, Cr^{met}, and Cr^{ox}. The oxide thickness by XPS is approximately 35 nm. Mass gain gives an average oxide thickness of 30nm (see Table 2).

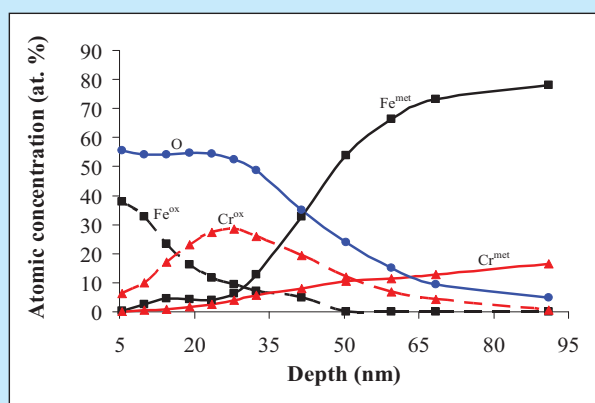


Figure 11
XPS depth profile of Fe-18Cr after 1 hour exposure in wet O₂ at 600°C showing the elemental distribution of O, Fe^{met}, Fe^{ox}, Cr^{met}, and Cr^{ox}. The oxide thickness by XPS is approximately 45 nm.

Table 3
Summary of phases identified by XRD

Alloy Comp.	Dry O ₂			Wet O ₂		
	1 hour	24 hours	168 hours	1 hour	24 hours	168 hours
Fe-2.25Cr	H, S	H, S	H, S	H, S	H, S	H, S
Fe-10Cr	C, α	C, α	C, α	H, S	H, S	H, S
Fe-18Cr	C, α	C, α	C, α	C, α	H, S	H, S
Fe-25Cr	C, α	C, α	C, α	C, α	C, α	H, S

H= Fe₂O₃ C= Cr rich (Fe,Cr)₂O₃ S= spinel = Fe₃O₄ and (Fe,Cr)₃O₄ (the two phases could not be distinguished because of peak overlap) α = the FeCr alloy substrate. The presence of a substrate peak (α) means that the oxide is quite thin (= protective).

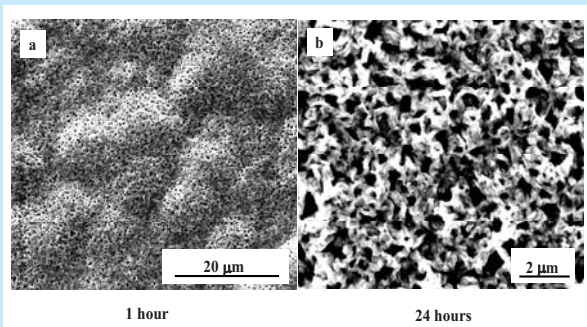


Figure 12
(a) and (b) shows plan view SEM images of the surface of Fe-2.25Cr after 1 and 24 hours in dry O₂ at 600°C.

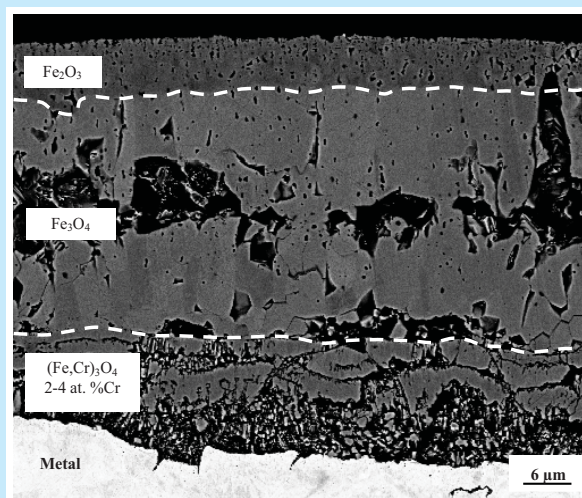


Figure 13
Manually polished cross section BSE image of Fe-2.25Cr after 168 hours in dry O₂ at 600 °C. Scale thickness is in the range 45-50 μm. The average scale thickness was about 40 μm according to mass gain (Table 2).

25Cr after 1 and 24 hours. In both cases the outer part of the oxide was poorer in chromium than in the corresponding exposures in dry O₂ (See Table 4). As expected, the chromium content in the oxide was generally higher for Fe-25Cr than for Fe-18Cr.

D. Morphology and Composition of the Scale in Dry O₂

Fe-2.25Cr

Fig. 12 shows plan view SEM images of the scale surface of Fe-2.25Cr after 1 and 24 hours exposure in dry O₂. Fig.13 shows a SEM cross section after 168 hours, showing that the scale is 45-50 μm thick and consist of three layers. According to a combination of EDX analysis (not shown) and XRD (see Table 3) it was concluded that the outermost layer consists of hematite (Fe₂O₃) while the middle layer is magnetite (Fe₃O₄) and the bottom layer is iron chromium spinel oxide (Fe, Cr)₃O₄ with a chromium content of 2-4 at. %. Small voids are evenly distributed in the hematite and magnetite layers while large voids occur only within the magnetite layer. Some of the large voids may have formed during polishing.

Fe-10Cr, Fe-18Cr and Fe-25Cr

Fig. 14 shows plan view SEM images of the surface of the thin and protective oxide formed on Fe-10Cr after 1 and 168 hours exposure in dry O₂ (compare Table 2). Analysis by XRD (see Table 3) showed that the oxide consists of the solid solution (Cr, Fe)₂O₃. The same scale composition and similar scale morphology was exhibited by Fe-18Cr and Fe-25Cr in this environment (see Fig. 15).

E. Morphology and composition of the scale in wet O₂

Fe-2.25Cr

The scale formed on Fe-2.25Cr in wet O₂ at 600°C suffered strong exfoliation during cooling. Investigation of the spalled scale by XRD and of the

scale remaining on the alloy by cross section SEM/EDX (not shown) showed that the scale had the same general composition and morphology as in the dry O₂ exposure, consisting of consecutive layers of hematite, magnetite and (Fe, Cr)₃O₄, the Cr content in the latter compound being a few percent (see Fig.13 for a cross section of the scale in dry O₂). The main difference between the exposures in dry and in wet O₂ is the appearance of blade-shaped hematite crystallites in the wet environment. The plan view SEM image in Fig. 16 of a part of the scale (which was not exfoliated) after 1 hour exposure in wet O₂ at 600°C shows hematite blades and nodules.

Fe-10Cr

The scale formed on Fe-10Cr after 1 hour exposure in wet O₂ is shown in the plan view

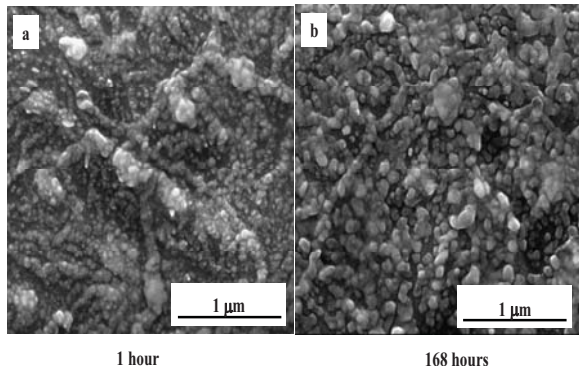


Figure 14
(a) and (b) shows plan view SEM images of the surface of Fe-10Cr after 1 and 168 hours exposure in dry O₂ at 600 °C. Average scale thickness is about 75 and 90 nm according to mass gain (see Table 2).

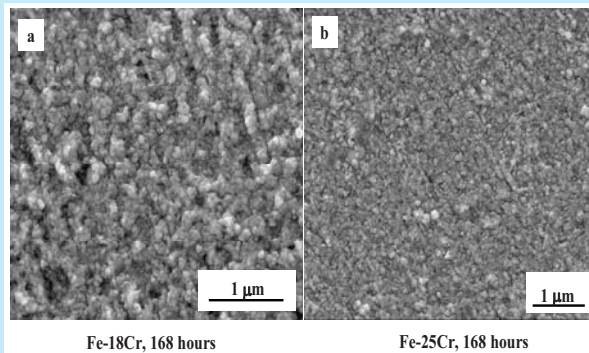


Figure 15
Plan view SEM images of Fe-18Cr (a) and Fe-25Cr (b) after 168 hours in dry O₂ at 600 °C. Average scale thickness was about 80 nm according to mass gain (see Table 2).

SEM images in Fig.17. The sample surface can be described in terms of a patchlike distribution of protective and non-protective oxide (see Figure 17 (a) and (b)). It may be noted that no spallation occurred in this case. In the backscattered electron mode image in Fig 17(b), the two types of surfaces show different contrast because of the great difference in oxide thickness. Thus, the bright areas correspond to a thin (and protective) oxide. The presence of two radically different types of oxide is also seen in the higher magnification images in Fig. 17(c)-(d). The non-protective scale exhibits a characteristic surface morphology with whiskers and blades as well as porous areas. Based on the combined evidence from XRD and SEM/EDX (not shown) it is concluded that

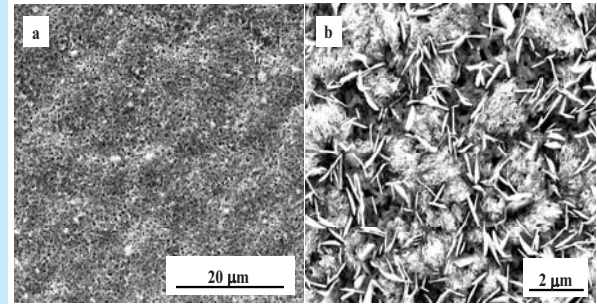


Figure 16
(a) and (b) shows plan view images using secondary electron of Fe-2.25 after 1 hour exposure at 600 °C in wet O₂. (The average scale thickness was about 8mm according to mass gain (Table 2).

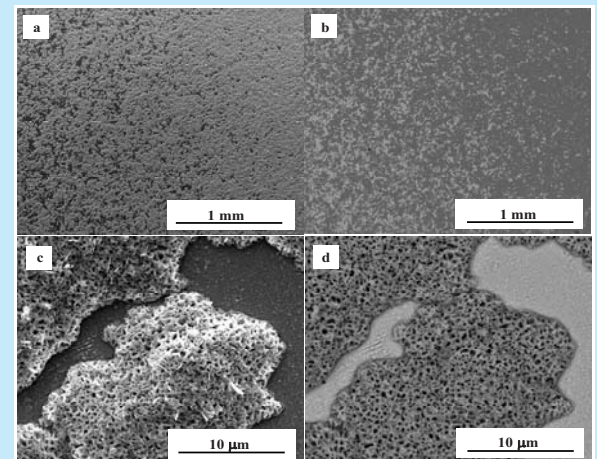


Figure 17
(a) and (b) shows secondary and backscattered electron plan view images of (c) and (d) at higher magnification of Fe-10Cr after 1 hour exposure at 600°C in wet O₂. The average scale thickness was about 5mm according to mass gain (Table 2).

these surface features consist of hematite. In contrast, the thin protective oxide is very similar to the oxide formed in dry O₂ (see Figure 17(e)). Based on this similarity and based on XRD (See Table 3) it is concluded that the thin oxide consists of corundum-type (Fe, Cr)₂O₃ of the type formed in dry O₂ (see above) After longer exposure times (24 and 168 hours) there is no protective oxide left on the surface. Fig. 18 shows the scale morphology after 24 and 168 hours, showing whiskers, blades and porous features on the scale surface. Fig. 19 shows a scale cross section of Fe-10Cr after 168 hours in wet O₂. The scale is made up of three layers, consisting of hematite (Fe₂O₃), magnetite (Fe₃O₄) and iron chromium spinel (Fe, Cr)₃O₄. The chromium level in the iron chromium spinel

at the bottom is about 8 at. %, corresponding to the stoichiometry (Fe_{0.8}Cr_{0.2})₃O₄. The magnetite layer contains many voids. The straight magnetite/spinel interface corresponds to the original metal surface. A close-up of the interface between the iron chromium spinel and the alloy is shown in Fig. 20. A reaction zone is observed at the scale/metal interface exhibiting a fishbone-like morphology. The reaction zone is a result of internal oxidation of the alloy and consists of a mixture of chromium rich oxide and iron rich metal. Fig. 21a illustrates the surface morphology of Fe-18Cr after 1 hour of exposure in wet O₂, showing the presence of a thin and protective (Fe, Cr)₂O₃ oxide (compare Tables 2, 3). Fig. 21b shows the same material after 24 hours in wet O₂. At this stage breakaway oxidation has occurred in a very rough surface with hematite blades and nodules. Fig.

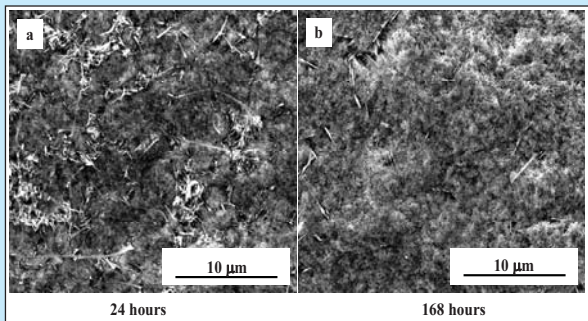


Figure 18
Plan view SEM image showing the scale surface on Fe-10Cr after 24 and 168 hours in wet O₂ at 600 °C. The average scale thickness was about 30mm (24 hours) and 68mm (168 hours) according to mass gain (Table 2).

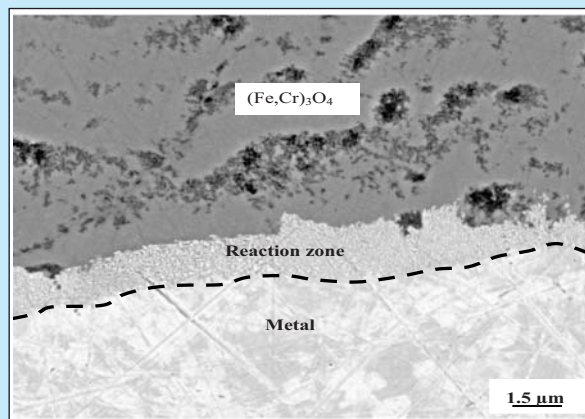


Figure 20
Close-up of region marked in Fig. 19 showing the interface between the iron chromium spinel and the alloy on Fe-10Cr after 168 hours exposure in wet O₂ at 600°C.

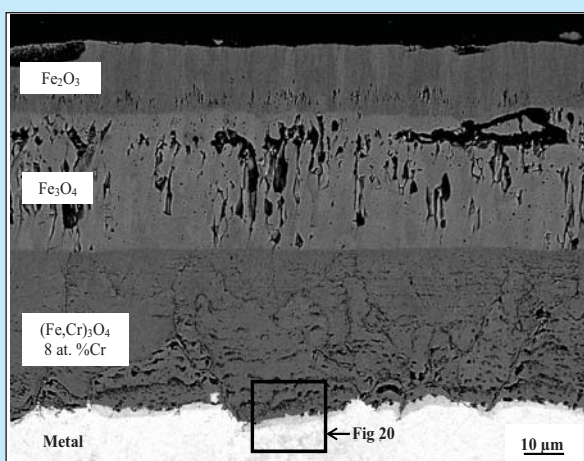


Figure 19
BSE image of cross section of Fe-10Cr after 168 hours exposure in wet O₂ at 600°C. Scale thickness is about 85 mm. The average scale thickness was 68 mm according to mass gain (Table 2).

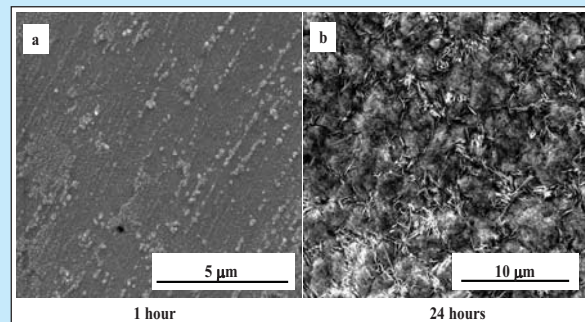


Figure 21
(a) Plan view SE images of Fe-18Cr after (a) 1 and (b) 24 hours in wet O₂ at 600°C. The average scale thickness in (b) was about 16mm according to mass gain (Table 2).

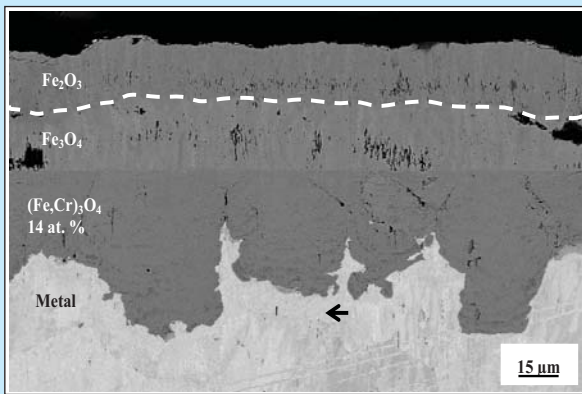


Figure 22
BSE image of manually polished cross section Fe-18Cr after 168 hours exposure in wet O₂ at 600°C. Scale thickness is in the range 50-90 mm. The average scale thickness was 55 mm according to mass gain (Table 2). Reaction zones (internal oxidation) are present at the scale alloy interface.

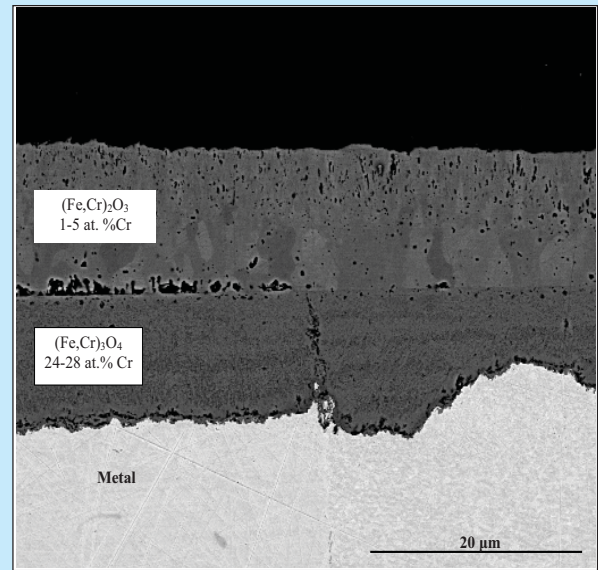


Figure 24
BSE image of cross section of Fe-25Cr after 168 hours exposure in wet O₂ at 600°C. The scale thickness in the image is in the range 18-24 mm. The average scale thickness was 11 mm according to mass gain (Table 2).

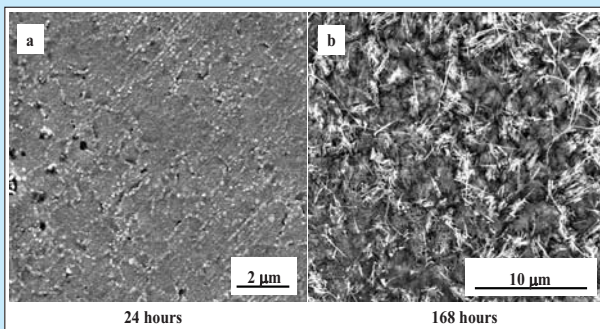


Figure 23
(a) Plan view images of Fe-25Cr after (a) 24 and (b) 168 hours in wet O₂ at 600°C. The average scale thickness in (b) was 11 mm according to mass gain (Table 2).

22 shows a cross section through the scale formed on Fe-18Cr after breakaway oxidation (168 hours in wet O₂). The scale is made up of three layers, consisting of hematite (Fe₂O₃), magnetite (Fe₃O₄) and iron chromium spinel. The iron chromium spinel at the bottom contains about 14 at. % of Cr, corresponding to Fe₂CrO₄. The straight magnetite/spinel interface corresponds to the original metal surface. The main differences in comparison to the scale formed on Fe-10Cr after breakaway are that the magnetite part of the scale contains fewer voids and that the scale/metal interface is very much rougher. A reaction zone was observed at the scale alloy interface also in this case. Like the other FeCr alloys, Fe-25Cr also suffers

breakaway oxidation in wet O₂ at 600°C. In this case, the thin oxide is more resilient, being replaced by a thick layered scale only after more than 24 hours exposure. The thin protective oxide present after 24 hours in wet O₂, consisted of corundum-type (Fe, Cr)₂O₃ and is shown in Fig. 23a (compare Table 3). XPS depth profiling (not shown) indicated that the oxide has a thickness of about 35 nm. After 168 hours, the protective oxide has transformed to a non-protective thick scale featuring blade and nodular hematite on the surface (see Fig. 23b). Fig. 24 shows a scale cross section after breakaway oxidation has occurred (see Fig. 24). Plan view imaging (not shown) indicated large variations in scale thickness in this case. This variation is suggested to account for the rather large difference between the thickness of the scale depicted in the image and the average scale thickness according to the mass gain. In this case the scale is duplex, the outer part consisting of hematite with 1-5 at % Cr (corresponding to (Fe_{0.98}Cr_{0.02})₂O₃ - (Fe_{0.88}Cr_{0.12})₂O₃) while the inner part is made up of (Fe, Cr)₃O₄ spinel. The Cr content varies in the range 24-28 at. % Cr (corresponding to Fe_{1.3}Cr_{1.7}O₄ - FeCr₂O₄). The straight interface between the two layers corresponds to the original surface. Voids are frequent in both layers, especially in the inner parts. As in the case of Fe-18Cr, the scale/metal interface is very rough. A reaction zone (internal oxidation) is present at

the scale metal interface also in this case but is less prominent than for Fe-10Cr and Fe-18Cr.

IV. DISCUSSION

The gravimetric results (Table 2), the microstructural characterization and the XRD analysis of the oxidized samples (Table 3) all show that the oxidation of the four alloys can be described in terms of two, radically different, types of behaviour. Thus, exposure in dry O_2 at $600^\circ C$ resulted in the formation of a thick, rapidly growing scale on Fe-2.25Cr while the three other alloys (Fe-10Cr, Fe-18Cr and Fe-25Cr) formed a thin ($<0.1\mu m$), protective oxide. Exposure to wet O_2 at the same temperature is considerably more demanding from the oxidation point of view, thick and poorly protective scales forming not only on Fe-2.25, but also on the other three alloys after an incubation period that depended on the chromium content. Thus, Fe-10Cr, Fe-18Cr and Fe-25Cr initially formed a thin and protective oxide which later converted into thick (about $5-50\mu m$) and poorly protective oxide (see for example Tables 2 and 4).

It is notable that the thick scales formed on the four alloys are quite similar. Thus, the thick scale on Fe-2.25Cr (wet and dry O_2) consisting of an outer hematite layer, a middle magnetite layer and a FeCr spinel oxide layer at the bottom is in principle the same as that formed on Fe-10Cr and Fe-18Cr (see for example Figs. 13, 19 and 22). Surprisingly, the mass gain (= average scale thickness) is also about the same (See Table 2). There are only minor differences between these scales, for example regarding the chromium concentration in the FeCr spinel oxide which is correlated to the alloy chromium content. The thick scale formed on Fe-25Cr after >24 hours exposure in wet O_2 differs somewhat from the others. Thus, it consists of two instead of three layers, there being no magnetite layer in the middle of the scale. All cross sections of thick scales exhibit a straight line in the middle of the scale (see Figs. 13, 19, 22, 24). It is considered that this interface corresponds to the original sample surface. Hence, the parts of the scale outside the sharp interface have grown by outward cation diffusion while the scale below the interface has grown by inward transport of oxygen. Hence, the magnetite and hematite formed on Fe-2.25Cr and on Fe-10Cr and Fe-18Cr after breakaway in wet O_2 have grown by outward diffusion of iron. Conversely, the $(Fe,Cr)_3O_4$ spinel present in the bottom of the scale on the same samples has grown

the inward growing spinel has almost reached its limiting composition in some areas, corresponding to $FeCr_2O_4$ (= chromite).

In contrast to the thick scale, the thin and protective oxide formed on Fe-10Cr, Fe-18Cr and

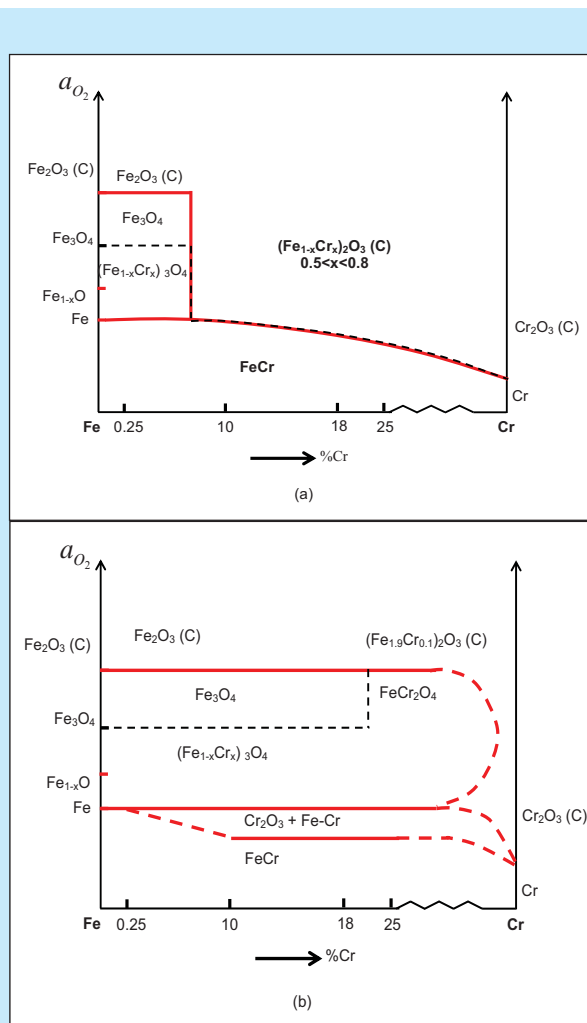


Figure 25

Experimental phase plot showing the oxides formed on Fe, Cr, and four FeCr alloys at $600^\circ C$ as a function of oxygen activity (the distance to the scale/metal and scale/gas interfaces) and of the composition of the metal (%Cr). (a) dry O_2 and wet O_2 , before breakaway. (b) wet O_2 after breakaway. The hatched line indicates the original interface, separating the oxides growing outward from those that grow inward.

by inward transport of oxygen ions. The absence of connected porosity in the scales allows us to rule out transport of oxygen in the form of gas molecules (O_2 or H_2O). In the case of Fe-25Cr, the outward growing scale consists of hematite containing some chromium ($Fe_{0.98}Cr_{0.02}O_3 - (Fe_{0.88}Cr_{0.12})_2O_3$), while

Table 4
Approximate composition by XPS of the thin and protective (Fe,Cr)₂O₃ oxide formed on Fe-10Cr, Fe-18Cr and Fe-25Cr after different exposure times in dry and wet O₂ at 600 °C

Alloy Comp.	Dry O ₂			Wet O ₂		
	1 hour	24 hours	168 hours	1 hour	24 hours	168 hours
Fe-10Cr						
Scale surface	Fe ₂ O ₃	-	(Fe _{0.8} Cr _{0.2}) ₂ O ₃	(B)	B	B
Bottom of scale	(Fe _{0.5} Cr _{0.5}) ₂ O ₃	-	(Fe _{0.4} Cr _{0.6}) ₂ O ₃	(B)	B	B
Fe-18Cr						
Scale surface	(Fe _{0.7} Cr _{0.3}) ₂ O ₃	(Fe _{0.6} Cr _{0.4}) ₂ O ₃	-	(Fe _{0.8} Cr _{0.2}) ₂ O ₃	B	B
Bottom of scale	(Fe _{0.4} Cr _{0.6}) ₂ O ₃	(Fe _{0.2} Cr _{0.8}) ₂ O ₃	-	(Fe _{0.3} Cr _{0.7}) ₂ O ₃	B	B
Fe-25Cr						
Scale surface	(Fe _{0.3} Cr _{0.7}) ₂ O ₃	(Fe _{0.3} Cr _{0.7}) ₂ O ₃	(Fe _{0.1} Cr _{0.9}) ₂ O ₃	-	(Fe _{0.4} Cr _{0.6}) ₂ O ₃	B
Bottom of scale	(Fe _{0.2} Cr _{0.8}) ₂ O ₃	(Fe _{0.2} Cr _{0.8}) ₂ O ₃	(Fe _{0.2} Cr _{0.8}) ₂ O ₃	-	(Fe _{0.2} Cr _{0.8}) ₂ O ₃	B

B= breakaway oxidation = very thick duplex oxide, no XPS analysis was performed (compare Tables 2 and 3)

Fe-25Cr in dry O₂ and initially in wet O₂ is single phase, consisting of the corundum-type solid solution (Fe_{1-x}Cr_x)₂O₃. The composition of the solid solution varies with exposure time and is correlated with the chromium content in the alloy. Also, the chromium content in the oxide generally increases as the scale metal interface is approached. The maximum chromium content in the thin protective oxide always corresponds to x > 0.5 (see Table 4). This may indicate the limiting chromium content for the thin oxide to remain stable at this temperature.

The transition from a thin protective oxide to a poorly protective, fast growing scale on Fe-10Cr, Fe-18Cr and Fe-25Cr in wet O₂ is termed breakaway oxidation. The gravimetric results and the microstructural characterization imply that the transition is sudden. The only case where both types of oxidation regimes occur simultaneously on one sample is for Fe-10Cr after 1 hour of exposure to wet O₂ (see Fig. 17).

The present observations regarding the phase composition of the scale at 600 °C are summarized in Fig. 25 a, b. The figure shows the oxide phases observed as a function of the activity of oxygen (the distance to the scale/metal and scale/gas interfaces) and of the composition of the alloy (%Cr). In addition to the four model alloys, data for pure iron and chromium is also included. Fig. 25a shows the phases observed under “mild” conditions, *i.e.* dry oxygen and short exposure times in wet O₂, while

Fig. 25 b shows the situation for the four alloys in wet O₂, after breakaway has occurred.

It may be noted that the thick hematite/magnetite/spinel scale formed on Fe-2.25Cr and on Fe10Cr and Fe-18Cr after breakaway in wet O₂, is similar to the scale formed on pure iron below the wüstite decomposition temperature. Thus, below about 570 °C iron forms a scale where the outer hematite layer is followed by two consecutive magnetite layers. The border between the two magnetite layers is reported to correspond to the original sample surface, the outer magnetite having formed by outward cation migration while the inner magnetite layer has formed by inward oxygen diffusion (Pujilaksono et al. 2008 & Ueda et al. 2005). Hence, the two outer layers of the scale are the same as for Fe10Cr and Fe-18Cr after breakaway while the inward growing magnetite is replaced by iron chromium spinel (Fe,Cr)₃O₄ on Fe-10Cr and Fe-18Cr. Above 570 °C, iron forms a scale where the innermost layer consists of wüstite (Fe_{1-x}O). Alloying with chromium decreases the stability of wüstite, explaining why it is no observed in the present study. There are also great similarities between the protective (Fe_{1-x}Cr_x)₂O₃ oxide formed on Fe-10Cr, Fe-18Cr and Fe-25Cr and the Cr₂O₃ film formed on pure chromium.

This study shows that oxidation behaviour of the model alloys is intermediate between that of the pure metals. Thus the oxidation of Fe-2.25Cr, and of Fe-10Cr, Fe-18Cr and Fe-25Cr after breakaway,

resembles the oxidation behaviour of pure iron while the thin protective oxide formed Fe-10Cr, Fe-18Cr and Fe-25Cr resembles the chromia layer formed on pure chromium. The rate of oxidation after breakaway is slightly lower than that of pure iron, the mass gains of Fe-2.25Cr and Fe-10Cr after 24 hours in wet O₂ being about 70% of that reported for pure iron in the same environment (Pujilaksono et al. 2008). It is suggested that the lower oxidation rate is due to the absence of wüstite on the FeCr alloys. The observation that the mass gain after 168 hours in wet O₂ is the same for Fe-2.25Cr and Fe-10Cr (Table 2) implies that the chromium concentration in the FeCr spinel layer does not influence the rate of oxidation. It may be noted that when the oxide is protective, the rate of oxidation of Fe-10Cr, Fe-18Cr and Fe-25Cr is less than for pure chromium. Thus, after 24 hours in dry O₂ at 600 °C the mass gain is about 30 µg/cm² for chromium (Pujilaksono et al. 2008) and 8-12 µg/cm² for the three FeCr alloys (Table 2). Also, while chromium exhibits strictly parabolic kinetics in dry O₂ (Pujilaksono et al. 2008) (k'' in dry O₂ at 600°C is reported to be $8.61 \cdot 10^{-15}$ g²/cm⁴s), the oxidation of Fe-10Cr, Fe-18Cr and Fe-25Cr is sub-parabolic.

As noted above, the corrosivity of the combination of water vapour and O₂ towards stainless steel has been attributed to the vaporization of CrO₂(OH)₂ from the oxidizing metal surface according to reaction (2) (see introduction). Thus, it was concluded that the protective properties of (Fe_{1-x}Cr_x)₂O₃ are weakened due to the resulting chromium depletion (Asteman 2002 & Asteman 2000). As a result, the material to go into breakaway oxidation, the thin oxide being replaced by a thick scale consisting of hematite and spinel oxide. The present investigation of binary FeCr alloys lends support to this view. Hence, the transformation of the thin protective oxide on e.g., Fe-18Cr into a thick and poorly protective oxide in wet O₂ is preceded by a decrease in the concentration of chromium in the protective oxide. This can be seen from a comparison of the composition of the protective oxide in dry and wet O₂ (see Figs.10 and 11 and Table 4). Interestingly, Fe-10Cr, Fe-18Cr and Fe-25Cr all respond to the presence of water vapour by going into breakaway oxidation. Hence, increasing the chromium concentration in the alloy does not stop the alloy from going into breakaway oxidation, it merely prolongs the incubation time.

Among the four alloys studied, Fe-2.25Cr is the only one that forms a thick scale in both wet and dry O₂ at 600 °C. The influence of water vapour on scale

morphology as shown by the formation of blade-shaped hematite crystallites at the scale surface in wet O₂ (compare Figs. 12 and 16) is closely paralleled by the influence of water on the oxidation of pure iron (Pujilaksono et al. 2008).

V. CONCLUSIONS

The oxidation behavior of the four FeCr alloys in dry and wet O₂ at 600 °C is intermediate between that of iron and chromium. The oxidation of Fe-2.25Cr is similar to iron in both environments, forming a poorly protective scale. Fe-10Cr, Fe-18Cr and Fe-25Cr form a thin protective oxide in some cases, similar to pure Cr, and a poorly protective oxide in other cases, being similar to iron. The poorly protective scales formed on Fe-2.25, Fe-10Cr and Fe-18Cr consist of three layers. The bottom part is made up of inward growing FeCr spinel while the middle and outer layers consist of outward growing magnetite and hematite, respectively. The slightly lower rate of oxidation compared to pure iron is attributed to the absence of wüstite on the FeCr alloys. Fe-25Cr develops a slightly different thick scale featuring no intermediate magnetite layer. In dry O₂, Fe-10Cr, Fe-18Cr and Fe-25Cr form a thin and protective (Fe,Cr)₂O₃ oxide similar to the chromia film formed by pure chromium. However, the oxide growth rate on Fe-10Cr, Fe-18Cr and Fe-25Cr is much less than on pure chromium. In wet O₂, Fe-10Cr, Fe-18Cr and Fe-25Cr initially form the same kind of protective oxide film as in dry conditions. After an incubation time that depends on alloy chromium content, all three alloys go into breakaway oxidation and form thick, poorly protective scales. Breakaway oxidation is triggered by the evaporation of CrO₂(OH)₂ from the protective (Fe,Cr)₂O₃ oxide.

REFERENCES

- B. Pujilaksono, T. Jonsson, M. Halvarsson, J. E. Svensson and L. G. Johansson, *Oxidation of Metals*, Accepted for publication, 25 June 2008.
- B. Pujilaksono, T. Jonsson, M. Halvarsson, J.-E. Svensson and L.-G. Johansson, submitted to *Corrosion Science*, (2008).
- B. Tveten, G. Hultquist and T. Norby, *Oxidation of Metals*, **51**, 221 (1999).
- C. S. Tedmon, *Journal of the Electrochemical Society*, **113**, 766 (1966).
- E. J. Opila, D. L. Myers, N. S. Jacobson, I. M. B. Nielsen, D. F. Johnson, J. K. Olminky and M. D. Allendorf, *Journal of Physical Chemistry A*, **111**, 1971 (2007).

H. Asteman, J. E. Svensson and L. G. Johansson, *Oxidation of Metals*, **57**, 193 (2002).

H. Asteman, J. E. Svensson, M. Norell and L. G. Johansson, *Oxidation of Metals*, **54**, 11 (2000).

M. Hansel, W. J. Quadackers and D. J. Young, *Oxidation of Metals*, **59**, 285 (2003).

M. Ueda, K. Kawamura and T. Maruyama, In: *High-*

Temperature Oxidation and Corrosion 2005, p. 37 (2005).

N. Birks, G. H. Meier and F. S. Pettit, *Introduction to the High-Temperature Oxidation of Metals*, Cambridge University Press (2006).

P. Kofstad, *High Temperature Corrosion*, Elsevier Applied Science, New York (1988).